

Diamond Refractive Optics for modern X-ray sources

© I. Snigireva,¹ A. Snigirev²✉

¹European Synchrotron Radiation Facility,
38043 Grenoble, France

²Immanuel Kant Baltic Federal University,
236041 Kaliningrad, Russia

✉e-mail: anatoly.snigirev@gmail.com

Received October 17, 2024

Revised October 17, 2024

Accepted October 17, 2024

The potential of creating diamond refractive optics using various diamond processing technologies, including microelectromechanical systems technology, laser cutting, and ablation, as well as ion-beam lithography was demonstrated. Experimental studies of lens samples were conducted at synchrotron and laboratory X-ray sources.

Keywords: diamond, compound refractive lenses, laser cutting, laser ablation, ion-beam lithography, focusing, imaging.

DOI: 10.61011/TP.2025.03.60843.323-24

Introduction

The emergence of third-generation synchrotron radiation sources has stimulated rapid development in both existing and new experimental methods related to coherence, such as phase-contrast and diffraction imaging, interferometry, X-ray microscopy, and coherent correlation spectroscopy [1–2]. The high degree of coherence, brightness, and power of the radiation has necessitated the development of optics using new materials that can withstand extreme thermal and radiation loads while maintaining beam coherence. Special attention should be given to improving optics with the advent of fourth-generation sources featuring diffraction-limited beams.

One of the most prominent examples of successful advancements in X-ray optics is compound refractive lenses (CRLs), first proposed 25 years ago [3]. Today, X-ray CRLs have become a key tool at modern synchrotron facilities due to their ease of use and high versatility. By modifying the shape, composition, and number of individual lenses, X-ray CRLs can be adapted to photon energies in the range of 2–200 keV, allowing flexible focal length adjustment from fractions of a millimeter to hundreds of meters for a wide variety of applications. Refractive optics can be used for beam transport and shaping, functioning as condensers, collimators, higher harmonic filters, etc. [4–11]. CRLs are widely applied in X-ray microscopy, interferometry, Fourier optics, and spectroscopy [12–25].

X-ray optical materials with minimal absorption, maximum refractive power, and high thermal and mechanical stability are of great interest for new radiation sources. If we use the ratio of the decrement of the refractive index δ to the total linear attenuation coefficient μ to describe the optical properties of a material, the best-performing materials are aluminum (Al), diamond (C), and beryllium (Be). Currently, Be is the most widely used material for refractive lenses due to its high transparency

to X-rays. However, commercially available beryllium is a sintered granular material that causes significant parasitic scattering of X-ray radiation at grain boundaries, voids, inclusions, and other defects, which significantly degrades the focusing and imaging quality of the lenses. Single crystals or amorphous materials are preferable for lenses, as they prevent radiation from „sensing“ the material’s internal structure.

Single crystalline carbon in the form of a diamond is an ideal choice. For example, at an energy of 10 keV, the δ/β ratio for diamond is 1000, which is quite high and not much lower than that of beryllium (4000). However, the δ value for diamond is twice that of beryllium, meaning that half as many lenses is required to achieve the same focal length with identical lens geometry. It should be noted that there are three types of X-ray radiation: a white beam directly from the source, a monochromatic beam using a monochromator, and the so-called pink beam — a beam reflected by a mirror to suppress higher harmonics. Diamond is the optimal material for use with all types of radiation due to its high-temperature stability, high thermal conductivity (κ), low thermal expansion coefficient (α), and chemical inertness. Thermo-mechanically, materials can be ranked by the κ/α coefficient [26–27], and at room temperature, the κ/α ratio for diamond is 100 times better than for beryllium. This high coefficient gives diamond excellent thermal and X-ray stability in monochromators subjected to high thermal loads in synchrotrons and X-ray free-electron lasers (XFELs) [27–31]. It is worth noting that beryllium lenses require more powerful cooling to prevent material recrystallization and lens profile deformation [32].

Despite all the advantages of diamond as a material for refractive lenses, a major barrier to its use is the difficulty of processing it: diamond is the hardest material in the periodic table and extremely chemically inert. Over the past few decades, various attempts have been made to fabricate diamond lenses using microelectromechani-

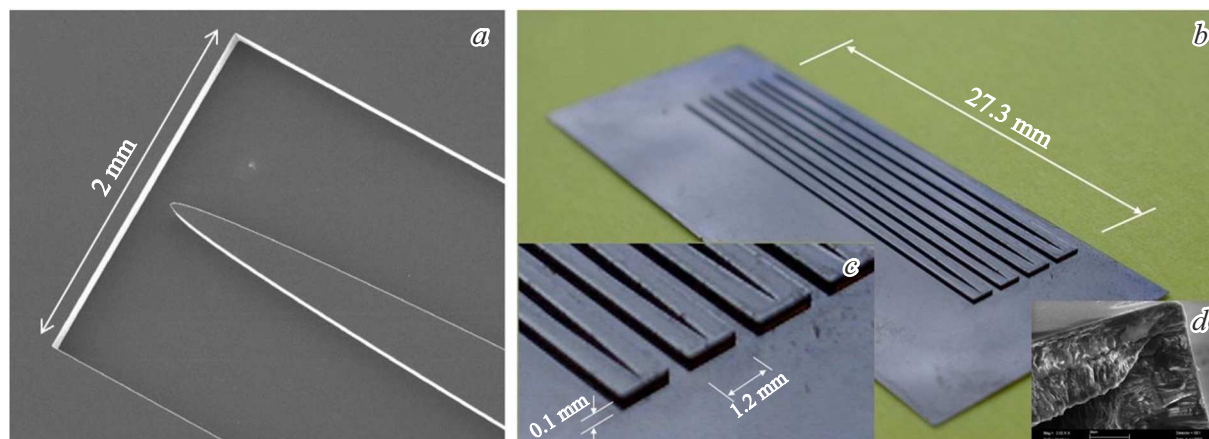


Figure 1. (a) Scanning electron microscope (SEM) image of the Si mold. (b-c) Photographs of the diamond lens at different magnifications. The lens parameters were as follows: parabola radius — $5\ \mu\text{m}$, lens length — $27\ \text{mm}$, lens height — $100\ \mu\text{m}$, lens aperture — $1\ \text{mm}$. (d) SEM image of the cross-section of the CVD diamond lens.

cal systems (MEMS) technology, including electron-beam lithography followed by reactive ion etching. The advent of lasers with ultrashort pulses ($< 10\ \text{ps}$) has enabled diamond processing using cutting and ablation technology. Moreover, it has been demonstrated that ion-beam lithography with direct material profiling can be successfully applied to fabricate diamond microlenses.

In this review, we present the most successful implementations of diamond lenses, considering their optical properties and applicability for both synchrotron radiation and laboratory X-ray sources.

1. One-dimensional diamond lenses fabricated using planar MEMS technology

The first diamond refractive lenses were produced using the transfer molding method, which involves growing diamonds on a pre-patterned silicon wafer (mold) [33]. After the chemical removal of the mold, free-standing diamond films were obtained, with a copy of the original pattern being formed on the nucleation side of the diamond film. The silicon molds were created using silicon MEMS techniques, including photolithography and deep plasma etching (Fig. 1, a). Diamond films were deposited using the microwave plasma chemical vapor deposition (CVD) method with CH_4/H_2 gas mixtures. Before deposition, the molds were seeded with $5\ \text{nm}$ diamond particles in an ultrasonic bath to ensure a high density of nucleation sites. The lenses were designed for a $50\ \text{cm}$ focal length at an X-ray energy of $9\ \text{keV}$, with their parameters shown in Fig. 1, a-d.

The optical properties of these lenses were investigated at the ESRF ID15 and ID22 undulator beamlines using monochromatic, pink, and white X-ray beams in the $6\text{--}40\ \text{keV}$ energy range. The focused beam sizes were ap-

proximately: $2\text{--}4\ \mu\text{m}$ for the monochromatic beam, $\sim 8\ \mu\text{m}$ for the pink beam, and $35\ \mu\text{m}$ for the white beam. After 12 hours of exposure to the pink beam, no degradation in lens performance was observed. Lens stability was further confirmed after 16 hours of exposure to the white beam. In still air, the lens temperature stabilized at $40\ ^\circ\text{C}$ within 15 minutes. Numerical simulations showed that a planar parabolic diamond lens can withstand an incident power flux of up to $500\ \text{W}/\text{mm}^2$ without degradation.

Due to the nature of the fabrication process, these lenses had a polycrystalline structure. Compared to silicon planar lenses [34–35], the tested diamond lenses exhibited significant intensity losses in the focused beam due to low-angle scattering and polycrystalline diffraction. The obtained focal spot images revealed additional satellite spots near the main focus, caused by low-angle scattering [33]. Additionally, small polycrystalline diamond grains ($< 10\ \mu\text{m}$) and nanocrystalline diamond ($5\ \text{nm}$) at the diamond-mold interface during the early growth stages (Fig. 1, d) led to reduced thermal conductivity compared to monocrystalline diamond.

This fabrication method was also applied to produce nano-focusing lenses with small apertures, using polycrystalline and nanocrystalline diamond [36–38]. These lenses demonstrated improved quality and uniformity, achieving a focusing resolution of $210\ \text{nm}$ at an X-ray energy of $11\ \text{keV}$. However, the maximum lens depth in this case was only $\sim 30\ \mu\text{m}$, which is significantly less than what is required for practical applications.

Another approach to fabricating diamond lenses involved electron-beam lithography and reactive ion etching [39–41]. However, the desired focusing characteristics were not achieved due to low lens quality at both fabrication stages. Significant aberrations were observed due to lens shape distortions caused by lithography. Additional scattering was generated by surface roughness, resulting from an imperfect

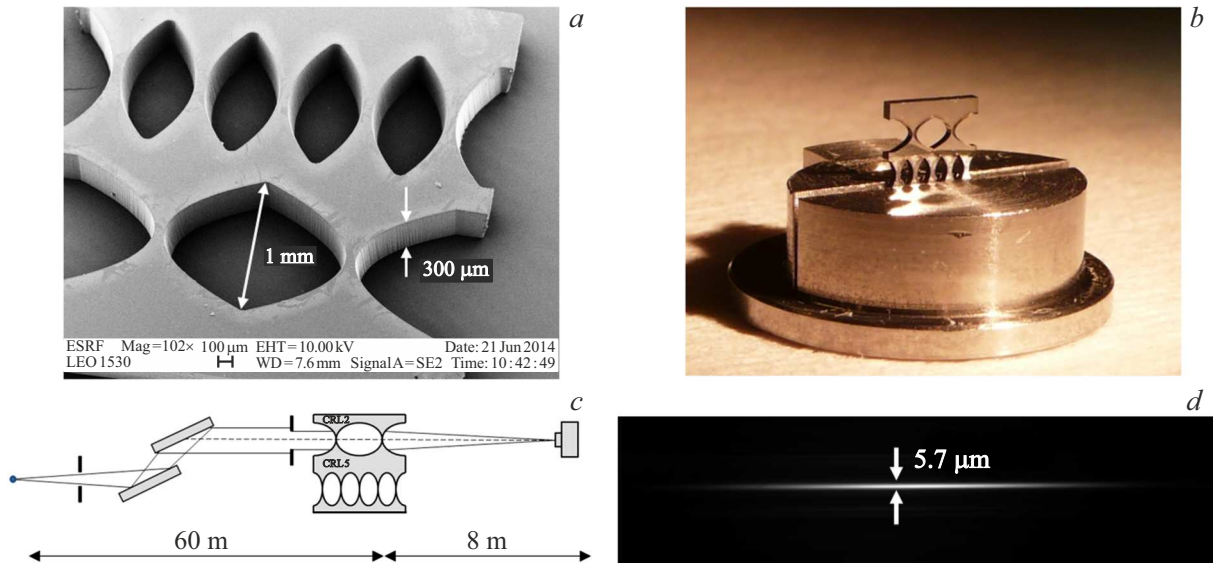


Figure 2. (a) SEM image of a diamond lens fabricated using laser cutting technology. (b) CRLs clamped in holders for X-ray testing. (c) Schematic of the experimental setup for ID06 measurements. (d) X-ray image of the focal line obtained for a CRL with two individual lenses. The horizontal size of the image is $300\ \mu\text{m}$, which corresponds to the thickness (depth) of the diamond plate ($3 \times 3\ \text{mm}^2$). The vertical width of the focal line is $5.7\ \mu\text{m}$ (FWHM), which is close to the initial source size of $40\ \mu\text{m}$.

etching process. Furthermore, these planar lenses were also fabricated with a very limited depth ($< 40\ \mu\text{m}$) [39].

2. One-dimensional diamond lenses fabricated by laser cutting

Over the past decade, the processing of diamonds using ultrashort laser pulses has seen significant development. Lasers enable precise diamond cutting without leaving cutting edges. Laser cutting prevents material deformation because the thermal load is confined to a small volume. For this reason, the creation of diamond lenses based on laser-cutting technology has been proposed.

The first large-aperture lenses [42] were fabricated using commercially available single crystal diamond plates. These plates were grown by chemical vapor deposition (CVD) and supplied by Element Six Ltd. The parabolic lenses were manufactured by „Micro Usinage Laser“ (Grattentour, France) using an Nd-YAG laser (355 nm) with precision galvanometric beam control synchronized with the movement of the diamond substrate. Two types of compound refractive lenses (CRLs) with varying numbers of individual lenses were laser-cut into the diamond plate: one row consisted of two individual lenses with a parabolic apex radius of $200\ \mu\text{m}$; the second row contained five individual lenses with a parabolic radius of $500\ \mu\text{m}$. The geometric aperture of both CRLs was 1 mm, and the depth of the structures was equal to the $300\ \mu\text{m}$ thickness of the diamond plate. The remaining diamond thickness between the apexes of adjacent parabolas was $75\ \mu\text{m}$. This value can be significantly reduced, but for initial tests, a conservative approach was taken to ensure the mechanical strength of the

sample. Scanning electron microscopy (SEM), presented in Fig. 2, a, showed good quality of the lens sidewalls, although some surface roughness was observed at the apex of the parabolas.

These diamond linear CRLs were tested at the micro-optics testing station of the undulator beamline ID06 (ESRF). A detailed description of the experiment can be found in [42], while only the key results are presented here. The vertical and horizontal source sizes were $40\ \mu\text{m}$ and $900\ \mu\text{m}$ (full width at half maximum, FWHM), respectively. Fig. 2, b shows the CRLs mounted in a holder for X-ray testing. The CRLs were positioned at a distance $L_1 = 60\ \text{m}$ from the source and oriented to focus monochromatic radiation in the vertical direction (Fig. 2, c). The efficiency of the CRLs and the focal spot size were measured using a high-resolution X-ray CCD camera (pixel size $0.64\ \mu\text{m}$) in the energy range of 7 to 12 keV. The measurement results for the CRL consisting of 2 lenses at 10 keV are shown in Fig. 2, d. At this energy, the image distance L_2 was 8 m, providing a source demagnification factor of $\times 7.5$. The vertical image size was $5.7\ \mu\text{m}$ (FWHM), corresponding to the effective X-ray source size of $40\ \mu\text{m}$, as measured using a boron fiber interferometer [43]. The uniform intensity of the focused beam images indicates the high quality of the lens sidewalls and their good verticality. The focal depth was approximately several centimeters. The intensity gain factor G , defined as the integrated intensity in the focal plane divided by the integrated intensity from the same area without the lens in the beam path (as described in [3]), was measured. Unfortunately, the measured intensity gain factor of 35 was half of the calculated value, which can

be attributed to parasitic scattering caused by the surface roughness of the lenses. Since the laser operated in a pulsed mode and the beam movement was not entirely continuous, a significant amount of material evaporated at stopping points, creating an unwanted comb-like lens profile.

As expected, the intensity gain factor for the CRL with 5 lenses was lower than that of the CRL with 2 lenses due to the presence of more individual lenses (resulting in more surfaces and junctions).

The experimentally obtained intensity gain factor can be used to estimate surface roughness. The theoretical value of G was calculated as described in [44] using the formula: $G = \frac{AT_p}{B_v}$ with $T_p = \frac{1}{A} \sqrt{\frac{\pi R}{\mu N}} e^{-\mu N d} e^{-2N(\frac{2\pi\delta}{\lambda}\tau)^2}$, where A is the physical aperture of the lens, B_v is the vertical size of the focused image, T_p is a transmission of the parabolic CRL, N is the number of biconcave elements, μ is the linear absorption coefficient, d is the websize of the biconcave lens, δ is the refractive index decrement, λ is the wavelength of the X-radiation and τ is the rms surface roughness. Since the discrepancy between theoretical and experimental values of G is mainly due to surface roughness, it can be easily estimated. For $\tau = 1.3 \mu\text{m}$, the calculated intensity gain factor matches the experimentally obtained value.

To improve surface roughness, the use of lasers with increased pulse frequency was proposed, as this results in a smoother distribution of deposited energy in the material. In [45–46], femtosecond lasers with a wavelength of 1030 nm and a high repetition rate were used to fabricate planar CRLs from polycrystalline CVD diamond plates with a thickness of $600 \mu\text{m}$ and a length of 8.5 mm. Three compound refractive lenses were fabricated in a single diamond plate: the first lens consisted of 3 single lenses with a parabolic apex radius of $50 \mu\text{m}$, the second lens consisted of 6 single lenses with a parabolic radius of $200 \mu\text{m}$, and the third lens consisted of 14 single lenses with a parabolic radius of $500 \mu\text{m}$. The distance between the apexes of adjacent parabolas was approximately $75 \mu\text{m}$.

Scanning electron microscopy (SEM) confirmed that the lens surfaces had submicron roughness ($0.3 \mu\text{m}$) and a slight vertical deviation angle of 1.7° . The focusing properties of the CRLs were tested using a MetalJet (ExcillumTM) microfocus X-ray source, which employs a liquid gallium jet as an anode. The source size was $20 \times 80 \mu\text{m}^2$ in the vertical and horizontal directions, respectively. Preliminary tests of the lenses for X-ray focusing (9.25 keV) demonstrated satisfactory performance. However, an increase in the focal spot size by $\sim 50\%$ (compared to the theoretical value for ideal parabolic geometries) was observed, which was attributed to the nonzero taper angle of the laser cut. Compared to previous studies [42] on diamond refractive lens fabrication using picosecond lasers, femtosecond laser processing enabled higher quality and smoother lens profiles. However, improving the verticality of the lens sidewalls remains critical and requires further refinement.

An attentive reader may notice that polycrystalline diamond was used in [45–46], despite previous statements

regarding the advantages of monocrystalline material. This choice was intentional — both for research purposes and to compare the manufacturing processes and optical characteristics of the two types of lenses.

The lenses described above had a key feature: they were fabricated from a single diamond plate. This can be considered both an advantage — simplifying lens alignment for experimental use — and a limitation — the lack of flexibility in choosing the number of lenses in the CRL. This can be critical for some applications, as the focal length of the CRL depends on the number of lenses and the energy of the X-ray radiation used. Therefore, it is sometimes necessary to use a CRL combined from individual diamond lenses, which are not physically connected to each other. For this purpose, linear individual cylindrical lenses were fabricated (Fig. 3, *a*) using commercially available monocrystalline diamond plates (Type IIa) grown by chemical vapor deposition (CVD) [47]. The cylindrical lens profiles were produced by Almax easyLab bvba (Belgium) using a picosecond Nd: YAG laser.

For experimental studies, individual lenses were assembled into a CRL configuration, as shown in Fig. 3, *b*. SEM imaging (Fig. 3, *c*) revealed an improved quality of the lens sidewalls, particularly in terms of surface roughness and verticality.

The assembled lenses were tested at the ID06 station (ESRF) [47]. The vertical size of the focal line matched the predicted value (according to the reduction factor). The uniformity of the linear focus in the horizontal direction indicates a high degree of verticality of the lens walls. The root-mean-square surface roughness was experimentally determined from the gain coefficient measurements and was found to be $1.2 \mu\text{m}$.

As can be seen, in this study, we significantly increased the depth of the lenses to 1.2 mm compared to the depth of $300 \mu\text{m}$ in the previous work [42]. However, further increasing the thickness and aspect ratio of the diamond lens will inevitably lead to a deterioration in the verticality of the lens side walls, resulting in significant focusing aberrations of the X-ray radiation. To overcome this issue, a modified fabrication geometry has been proposed, which allows the creation of even a two-dimensional parabolic profile. This approach will be presented in the next paragraph.

3. One-dimensional and two-dimensional diamond lenses manufactured by laser ablation technology

Currently, powerful lasers with ultra-short pulses in the picosecond and femtosecond ranges are available, allowing for the creation of precise three-dimensional structures via controlled layer-by-layer evaporation in laser ablation mode.

Two-dimensional [48] and linear [49] refractive lenses were fabricated at the Technological Institute of Superhard and New Carbon Materials (TISNUM, Russia, Troitsk) using the laser ablation method from high-quality synthetic

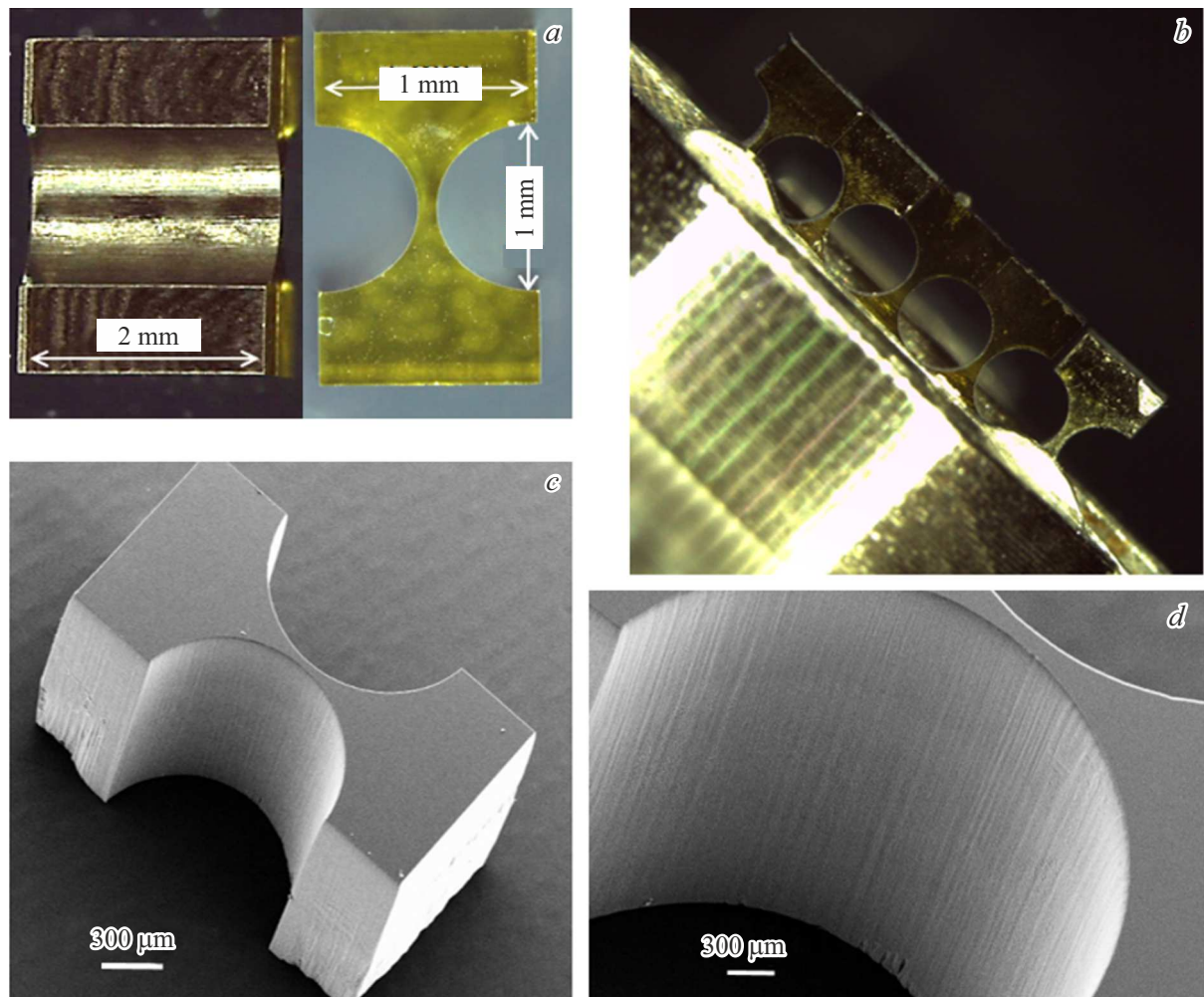


Figure 3. (a) Photographs of cylindrical lenses. Each lens has a curvature radius of $R = 500\ \mu\text{m}$ and a geometric aperture of 1 mm; the depth of the structures was equal to the thickness of the diamond plate, 1.2 mm. The thickness of the diamond between the peaks of consecutive cylinders was $100\ \mu\text{m}$. (b) Photograph of the assembly of five individual cylindrical lenses in a holder. (c) SEM image of the lens. (d) SEM image of the lens wall.

monocrystalline diamond material (type IIa). The substrate crystals were grown using the temperature gradient method under high pressure (5 GPa) and high temperature (1750 K) (HPHT) [50]. For one-dimensional lenses, the crystals were cut with a nanosecond laser into rectangular plates with the following dimensions: $500\ \mu\text{m}$ thickness, 2.5 mm length, and 1.5 mm width. For two-dimensional lenses, the crystals were cut into round disks with a thickness of $510 \pm 10\ \mu\text{m}$ and a diameter of 1.5 mm. The flat surfaces were mechanically polished to a micro-roughness of $\sim 5\ \text{nm}$. The profiles of the parabolic lenses were processed using a picosecond Nd: YAG laser (wavelength 355 nm) operating at the third harmonic. The laser beam, focused into a spot size of $10\ \mu\text{m}$, scanned across the plate, removing the diamond material layer by layer at a removal rate of $1\ \mu\text{m}$ per pass. The scanning pattern was adjusted for each layer to achieve a parabolic surface. With a pulse frequency of 500 kHz, the fabrication of a single lens took about 15 minutes. Fig. 4, a shows an SEM image of a two-

dimensional diamond lens manufactured by this method. To assess the lens profile and the radius at the top of the parabola, one lens was cut by laser along the rotational axis (Fig. 4, b). Measurements showed that the radius of the parabola at the lens edges was $R = 200\ \mu\text{m}$, and at the top of the parabola, the radius was close to $190\ \mu\text{m}$, indicating a relative radius error of 5%. The surface roughness at the top of the parabola, approximately $1\ \mu\text{m}$ (from peak to valley), was measured using an atomic force microscope.

SEM images of the linear parabolic diamond lens are shown in Fig. 4, c-d. Compared to previously tested lenses manufactured by laser cutting [42,45–46], the distinguishing features of the new lenses are the profile processing method and, consequently, the lens geometry; for instance, the one-dimensional profile has no limitations in aperture and lens width, nor in the profile depth. Unlike lenses cut from a single plate, the new lenses are free from the issue of non-perpendicular sidewalls.

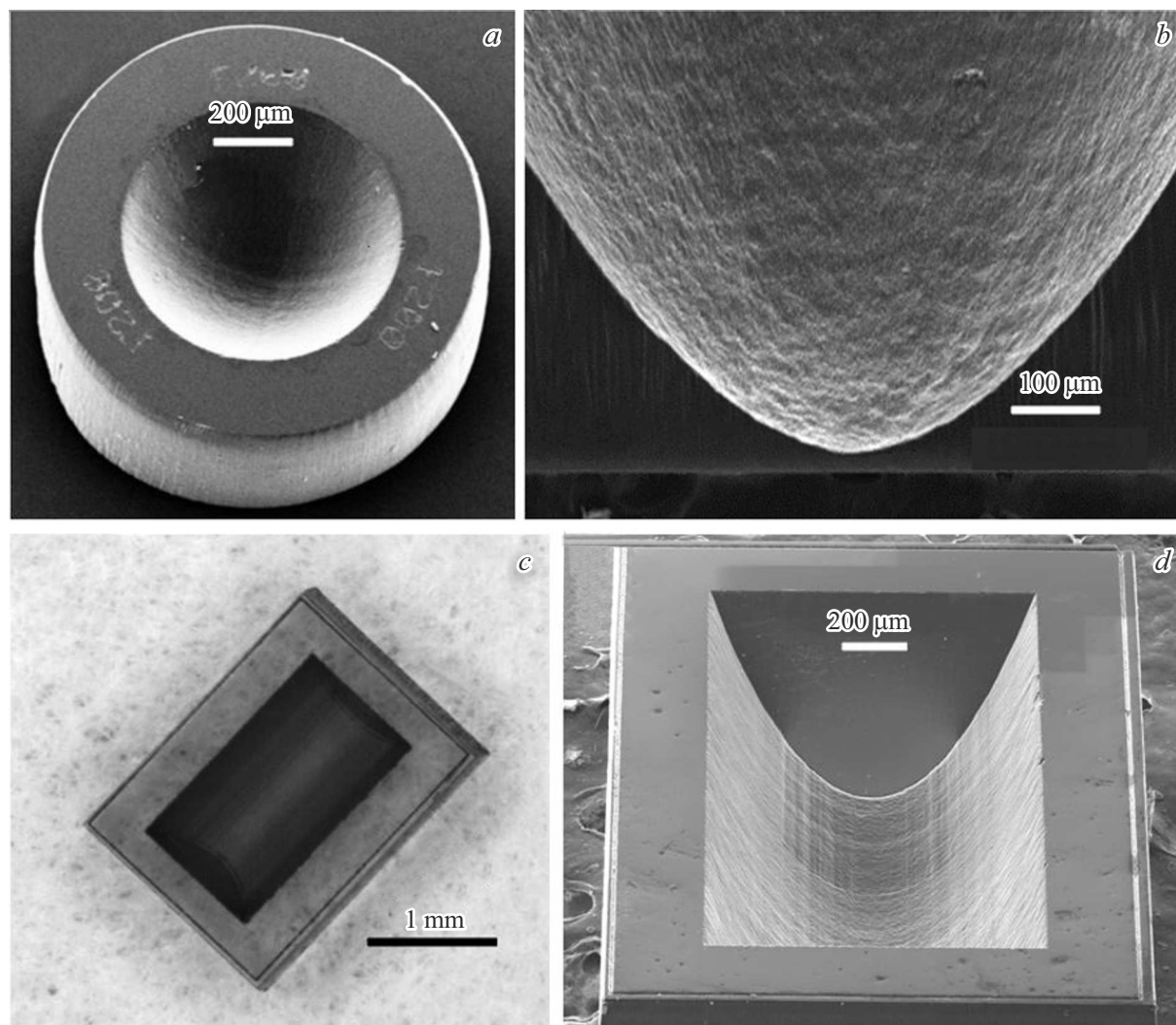


Figure 4. (a) SEM image of a 2-D diamond lens and (b) SEM image of the lens cut by laser along the rotation axis. The radius of curvature at the apex of the parabola was $R = 200\mu\text{m}$, the geometric aperture was $A \sim 1\text{ mm}$, and the thickness of the material at the apex of the parabola was $d = 30\mu\text{m}$. (c) Photograph of a 1-D diamond lens and (d) its SEM image. The radius of curvature at the apex of the parabola was $R = 200\mu\text{m}$, the geometric aperture was $A = 870\mu\text{m}$, the length was $L = 1.5\text{ mm}$, and the thickness of the material at the apex of the parabola was $d = 30\mu\text{m}$.

The lenses were tested both at synchrotron sources (ESRF and Argonne Photon Source) and at laboratory X-ray setups, including the Rigaku MultiMax-9 X-ray generator with a rotating anode and the MetalJet microfocus source using $\text{CuK}\alpha$ and $\text{GaK}\alpha$, respectively. Detailed experimental results obtained using X-ray imaging and focusing methods were published in works [48–49,51–52]. Experiments confirmed a relative error in the radius of 5–10%, thus aberration-free focusing was not achieved, and the focal line (for 1-D lenses) or the focal spot (for 2-D lenses) was slightly blurred. The surface roughness, evaluated through gain coefficient measurements, gave root-mean-square values of $\tau = 0.7\mu\text{m}$ for one-dimensional lenses and $\tau = 1.2\mu\text{m}$ for two-dimensional lenses. The latter value corresponds well to measurements obtained using an atomic force microscope.

It is worth noting that in work [53], femtosecond laser microprocessing was also used to fabricate two-dimensional lenses similar to those described in this section, with parabolas of small curvature radius ($\sim 105\mu\text{m}$) and a diameter of $450\mu\text{m}$, made in monocrystalline diamond plates obtained by chemical vapor deposition. Using one lens, the refocusing of a rotating magnet source to an almost Gaussian profile was demonstrated at a photon energy of 13.8 keV. A system of three lenses focused the radiation from an undulator into a spot size of $52\mu\text{m}$ (vertical) \times $21\mu\text{m}$ (horizontal) at an energy of 12 keV. The measured intensity gain factor of the system was 53, making such lenses suitable for tasks involving moderate focusing of high-power-density X-ray beams.

In [54], the authors conducted a thorough analysis of the thermal load and thermal properties of diamond and

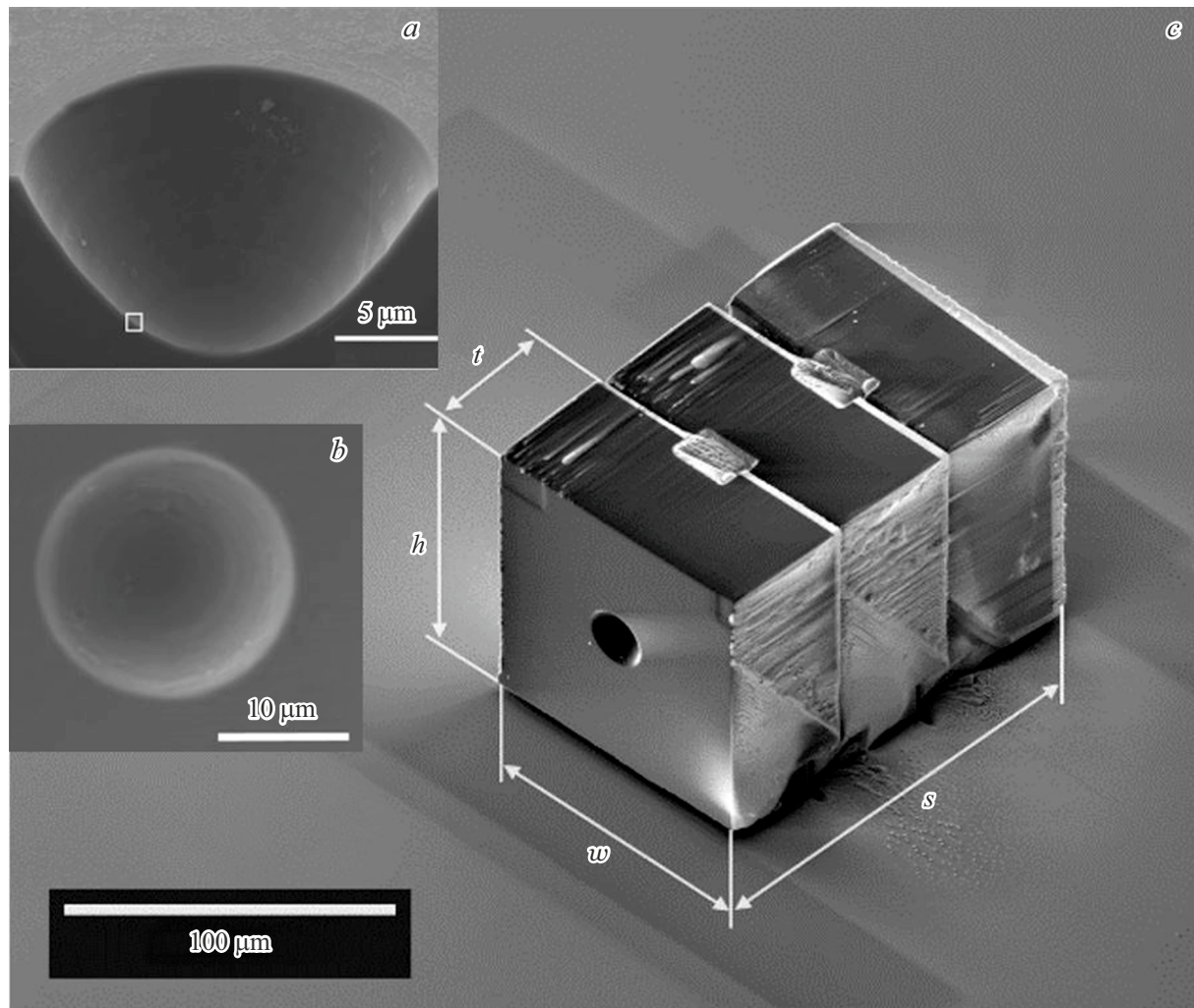


Figure 5. (a) Tilted (54°) SEM image of a microlens cut in half. (b) SEM image of a fabricated diamond microlens showing the roundness of the lens aperture. (c) SEM image of stacked diamond microlenses, demonstrating the precise positioning of individual half-lenses relative to each other. Dimensions are shown in isometry: the thickness t is $42\ \mu\text{m}$; the height h and width w are both: $w = h = 96\ \mu\text{m}$.

beryllium, which are common materials for X-ray refractive optics. It was found that the diamond lens heats up less than the equivalent beryllium lens at energies above 18 keV. Due to its lower coefficient of thermal expansion, the diamond lens can maintain its functionality in the lower energy range of 10–18 keV, despite experiencing a higher temperature rise compared to beryllium.

4. Two-dimensional diamond microlenses fabricated using ion-beam lithography

Despite the successful use of laser ablation, this method has significant limitations in terms of the quality of the lenses produced, as the laser beam typically has an irregular shape and uneven spatial energy distribution, which leads to severe radiation damage to the ablation surface. The lenses described earlier, to some extent, exhibited significant

micro-roughness on the surface and deviations from the parabolic shape of the designed profile. This prevented achieving a resolution better than 500 nm in microscopy mode [48–49]. Furthermore, laser ablation cannot produce lenses with radii smaller than $50\ \mu\text{m}$, which is necessary to reduce the diffraction limit of X-ray refractive optics.

To fabricate high-quality lenses with small radii, an alternative method for processing diamonds was proposed — ion-beam maskless lithography [55]. Ion-beam lithography allows for the formation of high-resolution three-dimensional surface profiles through the interaction of a finely focused ion beam (with a diameter down to 5 nm) with the sample. It has been demonstrated that ion-beam lithography can be applied to the fabrication of two-dimensional parabolic diamond microlenses, which are of great interest for nano-focusing X-rays and high-resolution microscopy.

Maskless direct „milling“ of diamond lenses was carried out using a Zeiss CrossBeam 540 FIB-SEM system equipped with a liquid gallium ion source. In-situ scanning electron microscopy (SEM) was used to control the shape and geometry of the fabricated samples. Two-dimensional diamond half-lenses were created in a monocrystalline diamond plate (100) with a thickness of $40\ \mu\text{m}$. The radius of curvature of one parabolic surface and the physical aperture were set to $5\ \mu\text{m}$ and $20\ \mu\text{m}$, respectively. The process of forming one half-lens took approximately 2.5 hours. As shown in the SEM image (Fig. 5, *a*), the lenses were almost free from pronounced low-frequency and high-frequency shape modulations, with a shape error of less than 200 nm and a surface roughness of 30 nm [55–56]. The SEM results also showed that the lens aperture has an almost ideal circular shape, further confirming the high accuracy of ion beam positioning (Fig. 5, *b*). Single lenses were assembled into a lens system (LSS) within a single technological process (Fig. 5, *g*) with high adjustment accuracy, which was further confirmed by X-ray phase-contrast imaging. The optical characteristics of the lens system were successfully tested at the P14 station, DESY, where diffraction-limited focusing of X-ray radiation was demonstrated, and Gaussian intensity profiles along the optical axis were shown.

Conclusion

This review demonstrates the potential of creating diamond refractive optics using various diamond processing technologies, including MEMS, laser cutting, and ablation, as well as ion-beam lithography. Experimental studies of lens samples were conducted at synchrotron and laboratory X-ray sources. Lenses fabricated using laser technologies have an average surface roughness of approximately $1\ \mu\text{m}$, which significantly limits their application at modern synchrotrons. Surface quality can be significantly improved through subsequent mechanical polishing methods [57–58] or using focused ion beams [56]. It is possible that laser water-jet technology for diamond processing will yield more promising results compared to traditional dry laser cutting and ablation methods. Currently, PALM Scientific is manufacturing diamond lenses by laser ablation with subsequent mechanical polishing [59]. Initial steps in the fabrication of diamond lenses for the PETRA III synchrotron are being taken at DESY [60]. As for microlenses made using the ion beam (FIB), they have a sufficiently smooth surface and can be used as objectives for dark-field X-ray microscopy [17].

With the launch and construction of 4th-generation synchrotrons, which provide virtually coaxially symmetric beams with extremely low divergence (~ 10 micro-radians), the use of diamond lenses as front-end optics for collimation and focusing appears extremely promising. Installed in the front-end (just after the radiation exits the undulators), such lenses will be able to capture and transmit the entire beam

to the experimental station with virtually no loss. Unlike beryllium, the ideal high thermo- and radiation resistance of diamond allows diamond optics to be used in white radiation almost without cooling. Moreover, single crystal diamond does not introduce undesirable diffuse scattering into the transmitted radiation.

However, optics made from perfect single crystal diamonds may present inconveniences in spectroscopy methods (EXAFS/XANES) when using extended spectral ranges. At certain X-ray energies, some crystal planes may be in the Bragg diffraction conditions, which leads to intensity loss, known as glitches, resulting in artifacts in measurements. The occurrence of glitches — parasitic Bragg reflections — was discussed in detail in [61–66].

An alternative to single crystals could be nanopolycrystalline diamond (NPD) [67–70], produced through the sintering process in a multi-anvil press under high pressures (~ 15 GPa) and temperatures ($\sim 2500\ ^\circ\text{C}$), through the direct transformation of pure graphite. The size of the diamond crystallites can vary widely from 10 to 100 nm.

Unfortunately, the unique technology for synthesizing nano-polycrystalline diamond is only implemented in Japan, where Sumitomo Electrical Industry manufactures cutting tools, and Ehime University provides anvils worldwide for high-pressure research. Given that Russia holds a leading position in the world in high-pressure physics and super-hard materials synthesis technologies, including diamonds, it would be advisable to develop domestic NPD technology, which will be highly demanded for the creation of synchrotron optics and scientific and technological instruments.

In this review, we aimed to familiarize the reader with the main and most significant trends in the field of diamond X-ray compound refractive optics, without claiming to provide a comprehensive citation of all works conducted in this area.

Acknowledgments

The authors express their gratitude to the team of the MNIC „Coherent X-ray Optics for Megascience Facilities“ at the Baltic Federal University.

Funding

The work was carried out with financial support from the Russian Federation, represented by the Ministry of Science and Higher Education, under Agreement № 075-15-2021-1350 dated October 5, 2021 (internal number 15.SIN.21.0004).

Conflict of interest

The authors declare that they have no conflict of interest.

References

- [1] R. Dimper, H. Reichert, P. Raimondi, L. Sanchez Ortis, F. Sette, J. Suzini. *Orange Book* (ESRF, Grenoble, France 2015), http://www.esrf.eu/Apache_files/Upgrade/ESRF-orange-book.pdf
- [2] A. Snigirev, I. Snigireva, V. Kohn, S. Kuznetsov, I. Schelokov. *Rev. Sci. Instrum.*, **66**, 5496 (1995). DOI: 10.1063/1.1146073
- [3] A. Snigirev, V. Kohn, I. Snigireva, B. Lengeler. *Nature*, **384**, 49 (1996). DOI: 10.1038/384049a0
- [4] A. I. Chumakov, R. Ruffer, O. Leopold, A. Barla, H. Thiess, T. Asthalter, B. P. Doyle, A. Snigirev, A. Q. R. Baron. *Appl. Phys. Lett.*, **77**, 31 (2000). DOI: 10.1063/1.126867
- [5] J.Y. Zhao, E.E. Alp, T.S. Toellner, W. Sturhahn, H. Sinn, D. Shu. *Rev. Sci. Instrum.*, **73**, 1611 (2002). DOI: 10.1063/1.1445823
- [6] G. B. M. Vaughan, J. P. Wright, A. Bytchkov, M. Rossat, H. Gleyzolle, I. Snigireva, A. Snigirev. *J. Synchrotron Rad.*, **18**, 125 (2011). DOI: 10.1107/S0909049510044365
- [7] A. Narikovich, M. Polikarpov, A. Barannikov, N. Klimova, A. Lushnikov, I. Lyatun, G. Bourenkov, D. Zverev, I. Panormov, A. Sinitsyn, I. Snigireva, A. Snigirev. *J. Synchrotron Rad.*, **26**, 1208 (2019). DOI: 10.1107/S1600577519005708
- [8] M. Polikarpov, I. Snigireva, A. Snigirev. *J. Synchrotron Rad.*, **21**, 484 (2014). DOI: 10.1107/S1600577514001003
- [9] A. Snigirev, I. Snigireva, M. Lyubomirskiy, V. Kohn, V. Yunkin, S. Kuznetsov. *Opt. Express*, **22**, 25842 (2014). DOI: 10.1364/OE.22.025842
- [10] M. Lyubomirskiy, I. Snigireva, V. Kohn, S. Kuznetsov, V. Yunkin, G. Vaughan, A. Snigirev. *J. Synchrotron Rad.*, **23**, 1104 (2016). DOI: 10.1107/S160057751601153X
- [11] D. Zverev, A. Barannikov, I. Snigireva, A. Snigirev. *Opt. Express*, **25**, 28469 (2017). DOI: 10.1364/OE.25.028469
- [12] M. Drakopoulos, A. Snigirev, I. Snigireva, J. Schilling. *Appl. Phys. Lett.*, **86**, 3 (2005). DOI: 10.1063/1.1843282
- [13] A. Snigirev, I. Snigireva, V. Kohn, V. Yunkin, S. Kuznetsov, M. Grigoriev, T. Roth, G. Vaughan, C. Detlefs. *Phys. Rev. Lett.*, **103**, 064801 (2009). DOI: 10.1103/PhysRevLett.103.064801
- [14] A. Bosak, I. Snigireva, A. Snigirev. *Adv. Mater.*, **22**, 3256 (2010). DOI: 10.1002/adma.201000173
- [15] P. Ershov, S. Kuznetsov, I. Snigireva, V. Yunkin, A. Goikhman, A. Snigirev. *J. Appl. Cryst.*, **46**, 1475 (2013). DOI: 10.1107/S0021889813021468
- [16] D. V. Byelov, J. M. Meijer, I. Snigireva, A. Snigirev, L. Rossi, E. van den Pol, A. Kuijck, A. Philipse, A. Imhof, A. van Blaaderen, G. J. Vroeghe, A. V. Petukhov. *RSC Adv.*, **3**, 15670 (2013). DOI: 10.1039/c3ra41223g
- [17] H. Simons, A. King, W. Ludwig, C. Detlefs, W. Pantleon, S. Schmidt, I. Snigireva, A. Snigirev, H. F. Poulsen. *Nat. Commun.*, **6**, 6098 (2015). DOI: 10.1038/ncomms7098
- [18] N. Dubrovinskaja, L. Dubrovinsky, N. A. Sapozhnikova, A. Abakumov, A. Tunner, M. Hanfland, E. Bykova, M. Bykov, C. Prescher, V. B. Prakapenka, S. Petitgirard, I. Chuvashova, B. Gasharova, Y. L. Mathis, P. Ershov, I. Snigireva, A. Snigirev. *Sci. Adv.*, **2**, e1600341 (2016). DOI: 10.1126/sciadv.1600341
- [19] K. V. Falch, D. Casari, M. Di Michiel, C. Detlefs, A. Snigirev, I. Snigireva, V. Honkimaki, R. Mathiesen. *J. Mater. Sci.*, **52**, 3497 (2017). DOI: 10.1007/s10853-016-0643-8
- [20] K. V. Falch, M. Lyubomirskiy, D. Casari, A. Snigirev, I. Snigireva, C. Detlefs, M. Di Michiel, I. Lyatun, R. Mathiesen. *Ultramicroscopy*, **184**, 267 (2018). DOI: 10.1016/j.ultramic.2017.10.001
- [21] M. Polikarpov, G. Bourenkov, I. Snigireva, A. Snigirev, S. Zimmermann, K. Csankó, S. Brockhauser, T. Schneider. *Acta Cryst.*, **D75**, 947 (2019). DOI: 10.1107/S2059798319011379
- [22] A. P. Chumakov, K. Napolskii, A. V. Petukhov, A. Snigirev, I. Snigireva, I. V. Roslyakov, S. V. Grigoriev. *J. Appl. Cryst.*, **52**, 1095 (2019). DOI: 10.1107/S1600576719011221
- [23] S. Lyatun, D. Zverev, P. Ershov, I. Lyatun, O. Kononov, I. Snigireva, A. Snigirev. *J. Synchrotron Rad.*, **26**, 1572 (2019). DOI: 10.1107/S1600577519007896
- [24] D. Zverev, I. Snigireva, V. Kohn, S. Kuznetsov, V. Yunkin, A. Snigirev. *Opt. Express*, **28**, 21856 (2020). DOI: 10.1364/OE.389940
- [25] D. Zverev, I. Snigireva, M. Sorokovikov, V. Yunkin, S. Kuznetsov, A. Snigirev. *Opt. Express*, **29**, 35038 (2021). DOI: 10.1364/OE.434656
- [26] A. M. Khounsary, R. K. Smither, S. Davey, A. Purohit. *SPIE*, **1739**, 628 (1992).
- [27] P. B. Fernandez, T. Graber, W. K. Lee, D. M. Mills, C. S. Rogers, L. Assoufid. *Nucl. Instr. Meth. Phys. Res. A*, **400**, 476 (1997). DOI: 10.1016/S0168-9002(97)01014-0
- [28] Yu. V. Shvyd'ko, S. Stoupin, A. Cunsolo, A. Said, X. Huang. *Nat. Phys.*, **6**, 196 (2010). DOI: 10.1038/nphys1506
- [29] J. Amann, W. Berg, V. Blank, F. J. Decker, Y. Ding, P. Emma, Y. Feng, J. Frisch, D. Fritz, J. Hastings, Z. Huang, J. Krzywinski, R. Lindberg, H. Loos, A. Lutman, H.-D. Nuhn, D. Ratner, J. Rzepiela, D. Shu, Yu. Shvyd'ko, S. Spampinati, S. Stoupin, S. Terentyev, E. Trakhtenberg, D. Walz, J. Welch, J. Wu, A. Zholents, D. Zhu. *Nat. Photon.*, **6**, 693 (2012). DOI: 10.1038/nphoton.2012.180
- [30] S. Stoupin, S. A. Terentyev, V. D. Blank, Yu. V. Shvyd'ko, K. Goetze, L. Assoufid, S. N. Polyakov, M. S. Kuznetsov, N. V. Kornilov, J. Katsoudas, R. Alonso-Mori, M. Chollet, Y. Feng, J. M. Glowina, H. Lemke, A. Robert, M. Sikorski, S. Song, D. Zhu. *Opt. Express*, **21**, 30932 (2013). DOI: 10.1364/OE.21.030932
- [31] S. Stoupin, S. A. Terentyev, V. D. Blank, Yu. V. Shvyd'ko, K. Goetze, L. Assoufid, S. N. Polyakov, M. S. Kuznetsov, N. V. Kornilov, J. Katsoudas, R. Alonso-Mori, M. Chollet, Y. Feng, J. M. Glowina, H. Lemke, A. Robert, M. Sikorski, S. Song, D. Zhu. *J. Appl. Crystallogr.*, **47**, 1329 (2014). DOI: 10.1107/S1600576714013028
- [32] L. Zhang, A. Snigirev, I. Snigireva, G. Naylor, F. Zontone, M. Di Michiel, P. Elleaume. *SPIE*, **5539**, 48 (2004). DOI: 10.1117/12.568105
- [33] A. Snigirev, V. Yunkin, I. Snigireva, M. Di Michiel, M. Drakopoulos, S. Kuznetsov. *SPIE*, **4783**, 1 (2002). DOI: 10.1117/12.451011
- [34] I. Snigireva, A. Snigirev, C. Rau, T. Weitkamp, V. Aristov, M. Grigoriev, S. Kuznetsov, L. Shabelnikov, Y. Yunkin, M. Hoffmann, E. Voges. *Nucl. Instrum. Methods A*, **467-468**, 982 (2001). DOI: 10.1016/S0168-9002(01)00556-3
- [35] A. Snigirev, I. Snigireva, M. Grigoriev, V. Yunkin, M. Di Michiel, S. Kuznetsov, G. Vaughan. *SPIE*, **6705**, 670506 (2007). DOI: 10.1117/12.733609
- [36] L. Alianelli, J. S. Sawhney, A. Malik, J. L. Fox, P. W. May, R. Stevens, I. M. Loader, M. C. Wilson. *J. Appl. Phys.*, **108**, 123107 (2010). DOI: 10.1063/1.3517060

- [37] A. M. Malik, O. J. Fox, L. Alianelli, A. M. Korsunsky, R. Stevens, I. M. Loader, M. C. Wilson, I. Pape, K. J. S. Sawhney, P. W. May. *J. Micromech. Microeng.*, **23**, 125018 (2013). DOI: 10.1088/0960-1317/23/12/125018
- [38] O. J. Fox, L. Alianelli, A. M. Malik, I. Pape, P. W. May, K. J. S. Sawhney. *Opt. Express*, **22**, 7657 (2014). DOI: 10.1364/OE.22.007657
- [39] B. Nohammer, J. Hoszowska, A. K. Freund, C. David. *J. Synchrotron Rad.*, **10**, 168 (2003). DOI: 10.1107/S0909049502019532
- [40] A. F. Isakovic, A. Stein, J. B. Warren, S. Narayanan, M. Sprung, A. R. Sandy, K. Evans-Lutterodt. *J. Synchrotron Rad.*, **16**, 8 (2009). DOI: 10.1107/S0909049508033736
- [41] M. Lyubomirskiy, P. Boye, J. M. Feldkamp, J. Patommel, S. Schoeder, A. Schropp, M. Burghammer, C. Wild, C. G. Schroer. *J. Synchrotron Rad.*, **26**, 1554 (2019). DOI: 10.1107/S1600577519007082
- [42] M. Polikarpov, I. Snigireva, J. Morse, V. Yunkin, S. Kuznetsov, A. Snigirev. *J. Synchrotron Rad.*, **22**, 23 (2015). DOI: 10.1107/S1600577514021742
- [43] V. Kohn, I. Snigireva, A. Snigirev. *Phys. Rev. Lett.*, **85**, 2745 (2000). DOI: 10.1103/PhysRevLett.85.2745
- [44] B. Lengeler, C. Schroer, J. Tummler, B. Benner, M. Richwin, A. Snigirev, I. Snigireva, M. Drakopoulos. *J. Synchrotron Rad.*, **6**, 1153 (1999). DOI: 10.1107/S0909049599009747
- [45] T. V. Kononenko, V. M. Gololobov, V. I. Konov. *Appl. Phys. A*, **122**, 258 (2016). DOI: 10.1007/s00339-016-9789-0
- [46] M. Polikarpov, T. V. Kononenko, V. G. Ralchenko, E. E. Ashkinazib, V. I. Konov, P. Ershov, S. Kuznetsov, V. Yunkin, I. Snigireva, V. M. Polikarpov, A. Snigirev. *SPIE*, **9963**, 9963OQ (2016). DOI: 10.1117/12.2238029
- [47] M. Polikarpov, I. Snigireva, A. Snigirev. *AIP Conf. Proceed.*, **1741**, 040024-1 (2016). DOI: 10.1063/1.4952896
- [48] S. Terentyev, V. Blank, S. Polyakov, S. Zholudev, A. Snigireva, M. Polikarpov, T. Kolpdziej, J. Qian, H. Zhou, Yu. Shvyd'ko. *Appl. Phys. Lett.*, **107**, 111108 (2015). DOI: 10.1063/1.4931357
- [49] S. Terentyev, M. Polikarpov, I. Snigireva, M. Di Michiel, S. Zholudev, V. Yunkin, S. Kuznetsov, V. Blank, A. Snigirev. *J. Synchrotron Rad.*, **24**, 103 (2017). DOI: 10.1107/S1600577516017331
- [50] S.N. Polyakov, V.N. Denisov, N.V. Kuzmin, M.S. Kuznetsov, S.Yu. Martyushov, S.A. Nosukhin, S.A. Terentiev, V.D. Blank. *Diamond Relat. Mater.*, **20**, 726 (2011). DOI: 10.1016/j.diamond.2011.03.012
- [51] M. Polikarpov, A. Barannikov, D. Zverev, S.A. Terentiev, S.N. Polyakov, S.I. Zholudev, S.Yu. Martyushov, V.N. Denisov, N.V. Kornilov, I. Snigireva, V.D. Blank, A. Snigirev. *SPIE*, **9964**, 99640J (2016). DOI: 10.1117/12.2238798
- [52] S.I. Zholudev, S.A. Terentiev, S.N. Polyakov, S.Yu. Martyushov, V.N. Denisov, N.V. Kornilov, M.V. Polikarpov, A. Snigirev, I. Snigireva, V.D. Blank. *AIP Conf. Proceed.*, **1764**, 020006 (2016). DOI: 10.1063/1.4961134
- [53] S. Antipov, S.V. Baryshev, J.E. Buyler, O. Antipova, Z. Liu, S. Stoupin. *J. Synchrotron Rad.*, **23**, 163 (2016). DOI: 10.1107/S1600577515020639
- [54] S. Antipov, S. Baryshev, S. Baturin, G. Chen, R. Kostin, S. Stoupin. *SPIE*, **9963**, 9963OR (2016). DOI: 10.1117/12.2238442
- [55] P. Medvedskaya, I. Lyatun, S. Shevyrtaiov, M. Polikarpov, I. Snigireva, V. Yunkin, A. Snigirev. *Opt. Express*, **28**, 4773 (2020). DOI: 10.1364/OE.384647
- [56] P. Medvedskaya, I. Lyatun, S. Shevyrtaiov, M. Polikarpov, I. Snigireva, V. Yunkin, A. Snigirev. *SPIE*, **11491**, 1149111 (2020). DOI: 10.1117/12.2568427
- [57] S. Antipov, E. Gomez, T. Roth, R. Selestre. *SPIE*, **11837**, 1183706 (2021). DOI: 10.1117/12.2595470
- [58] R. Selestre, S. Antipov, E. Gomez, T. Zinn, R. Barrett, T. Roth. *J. Synchrotron Rad.*, **29**, 629 (2022). DOI: 10.1107/S1600577522001795
- [59] <https://www.palm-scientific.com>
- [60] https://innovation.desy.de/technologies/diamondoptics/index_eng.html
- [61] M. Polikarpov, H. Emerich, N. Klimova, I. Snigireva, V. Savin, A. Snigirev. *Phys. Stat. Solidi B*, **255**, 1700229 (2018). DOI: 10.1002/pssb.201700229
- [62] Q. Zhang, M. Polikarpov, N. Klimova, H. B. Larsen, R. Mathiesen, H. Emerich, G. Thorkildsen, I. Snigireva, A. Snigirev. *J. Synchrotron Rad.*, **26**, 109 (2018). DOI: 10.1107/S1600577518014856
- [63] N. Klimova, O. Yefanov, I. Snigireva, A. Snigirev. *Crystals*, **11**, 504 (2021). DOI: 10.3390/cryst11050504
- [64] N. Klimova, I. Snigireva, A. Snigirev, O. Yefanov. *Crystals*, **11**, 1561 (2021). DOI: 10.3390/cryst11121561
- [65] N. Klimova, I. Snigireva, A. Snigirev, O. Yefanov. *J. Synchrotron Rad.*, **29**, 369 (2022). DOI: 10.1107/S1600577521013667
- [66] N. Klimova, A. Snigirev. *J. Surf. Investigations*, **17**, 1094 (2023). DOI: 10.1134/S102745102305021X
- [67] H. Sumiya, K. Harano, K. Arimoto, H. Kagi, S. Otake, T. Irifune. *Jpn. J. Appl. Phys.*, **48**, 120206 (2009). DOI: 10.1143/JJAP.48.120206
- [68] H. Ohfujii, T. Okuchi, S. Otake, H. Kagi, H. Sumiya, T. Irifune. *Diamond Related Mater.*, **19**, 1040 (2010). DOI: 10.1016/j.diamond.2010.02.015
- [69] T. Irifune, C. Ueda, S. Ohshita, H. Ohfujii, T. Kunimoto, T. Shinmei. *High Pressure Research*, **40**, 96 (2020). DOI: 10.1080/08957959.2019.1700981
- [70] I. Snigireva, T. Irifune, T. Shinmei, P. Medvedskaya, S. Shevyrtaiov, G. Bourenkov, M. Polikarpov, S. Rashchenko, A. Snigirev, I. Lyatun. *SPIE*, **11837**, 1183703 (2021). DOI: 10.1117/12.259467